ACSNANO
www.acsnano.org
ARTICLE

Excited State Biexcitons in Atomically Thin $MoSe_2$

Jiajie Pei,[†,‡] Jiong Yang,[†] Xibin Wang,[‡] Fan Wang,[§,∥] Sudha Mokkapati,[§] Tieyu Lü,[#] Jin-Cheng Zheng,[#] Qinghua Qin,[†] Dragomir Neshev,[⊥] Hark Hoe Tan,[§] Chennupati Jagadish,[§] and Yuerui Lu*[,†]

[†]Research School of Engineering, College of Engineering and Computer Science, [§]Department of Electronic Materials Engineering, Research School of Physics and Engineering, and [⊥]Nonlinear Physics Centre, Research School of Physics and Engineering, The Australian National University, Canberra, ACT 2601, Australia

[‡]School of Mechanical Engineering, Beijing Institute of Technology, Beijing 100081, China

[∥]ARC Centre for Nanoscale BioPhotonics (CNBP), Department of Physics and Astronomy, Faculty of Science, Macquarie University, Sydney, NSW 2109, Australia

[#]Department of Physics, and Collaborative Innovation Center for Optoelectronic Semiconductors and Efficient Devices, Xiamen University, Xiamen 361005, China

Supporting Information

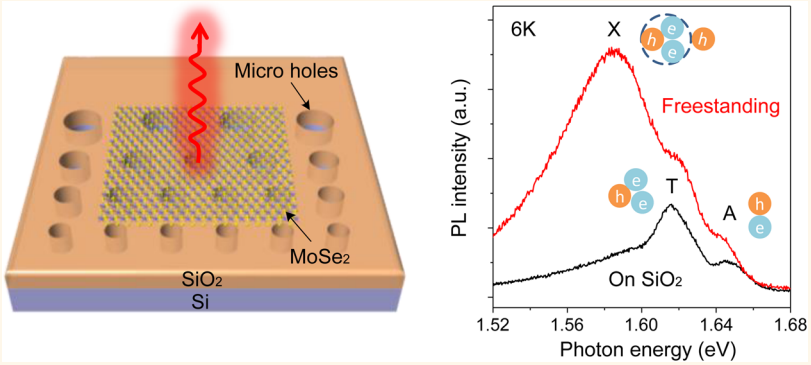

ABSTRACT: **The tightly bound biexcitons found in atomically thin semiconductors have very promising applications for optoelectronic and quantum devices. However, there is a discrepancy between theory and experiment regarding the fundamental structure of these biexcitons. Therefore, the exploration of a biexciton formation mechanism by further experiments is of great importance. Here, we successfully triggered the emission of biexcitons in atomically thin $MoSe_2$, *via* the engineering of three critical parameters: dielectric screening, density of trions, and excitation power. The observed binding energy and formation dynamics of these biexcitons strongly support the model that the biexciton consists of a charge attached to a trion (excited state biexciton) instead of four spatially symmetric particles (ground state biexciton). More importantly, we found that the excited state biexcitons not only can exist at cryogenic temperatures but also can be triggered at room temperature in a freestanding bilayer $MoSe_2$. The demonstrated capability of biexciton engineering in atomically thin $MoSe_2$ provides a route for exploring fundamental many-body interactions and enabling device applications, such as bright entangled photon sources operating at room temperature.**

KEYWORDS: *$MoSe_2$, biexciton, two-dimensional materials, freestanding, room temperature*

Atomically thin two-dimensional (2D) layered transition-metal dichalcogenide (TMD) semiconductors have aroused particular interest because of their interesting physical properties and promising applications in both fundamental research and optoelectronic devices.[1−7] The highly enhanced Coulomb interactions in these atomically thin layers, arising from the reduced dimensionality and weak dielectric screening, allow the formation of tightly bound excitons,[8] trions,[9,10] and biexcitons.[11−14] Biexcitons have been of particular interest for both fundamental studies of the remarkable many-body interactions[15−17] and investigations of novel device applications, such as quantum logic gates,[18] biexciton lasing devices,[19,20] entangled photon sources,[21] *etc.* Recently, tightly bound biexcitons have been observed in monolayer TMDs, such as WSe_2,[11] MoS_2,[12] and WS_2.[13] These biexcitons in monolayer TMDs show an ultralarge binding

Received: June 3, 2017
Accepted: July 3, 2017
Published: July 3, 2017

DOI: 10.1021/acsnano.7b03909
ACS Nano 2017, 11, 7468−7475

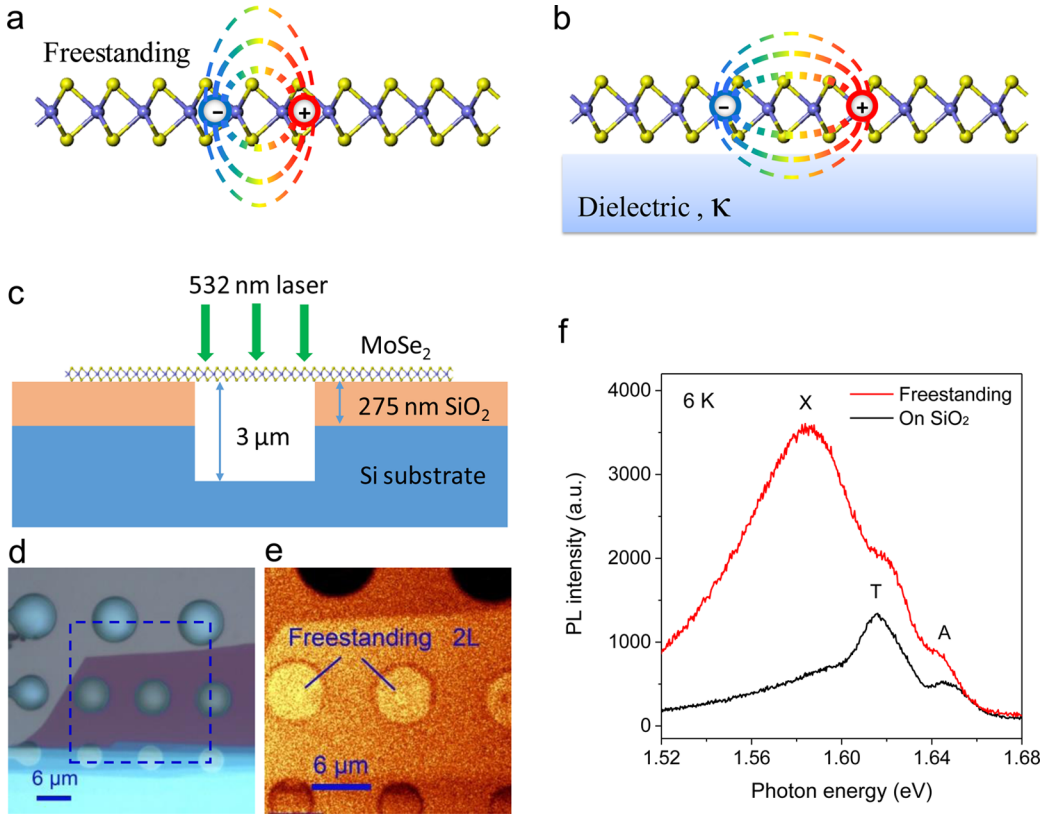

Figure 1. Photoluminescence (PL) of freestanding and dielectric-supported atomically thin $MoSe_2$. (a,b) Schematic representation of excitons (bound electron−hole pairs) for the freestanding (a) and dielectric-supported (b) monolayers. (c) Schematic cross section view of the device with freestanding $MoSe_2$. The $MoSe_2$ sample was mechanically transferred across circular holes that were prepatterned on a SiO_2 (275 nm)/Si substrate. The depth of the holes is 3 μm. (d) Optical microscope image of the freestanding bilayer (2L) $MoSe_2$ samples across 6 μm diameter holes. (e) PL mapping image of the region marked by the dashed square in (d). The holes covered by the freestanding sample are bright, whereas the holes without samples are dark. (f) Measured PL spectra from freestanding (red line) and SiO_2-supported (black line) 2L $MoSe_2$ at 6 K. The labels "A", "T", and "X" represent the emissions from excitons, trions, and a new emission peak, respectively.

energy in the range of 50−70 meV, which is more than 1 order of magnitude higher than the values found in III−V quasi-2D quantum wells.[22] This strong binding necessitates the complete understanding of the structures of these biexcitons and their dynamics in 2D materials as well as characterization of their properties and full investigation of their potential functionalities. A few theoretical models, such as the path integral Monte Carlo approach,[23] effective mass model,[24] and variational calculation method,[11] have been used to estimate the binding energies of biexcitons in TMD 2D materials. These models consider a biexciton to be a spatially symmetric four-particle state. However, based on this symmetric four-particle model, the predicted binding energies of biexcitons in TMD monolayers[11,23−25] are in the range of 18−24 meV, less than half of the values observed,[11−13] suggesting a discrepancy between theory and experiment. Recently, Varga *et al.*,[25] using high-accuracy variational calculations, showed that the predicted binding energies of excited state biexcitons in TMD monolayers are in the range of 50−70 meV, which agrees well with the earlier experimental data.[11−13] In Varga's model,[25] the excited state biexciton corresponds to a charge attached to a trion, which is energetically favorable than the ground state biexciton consisting of four spatially symmetric particles. How to further experimentally confirm the existence of the trion-charge-bound excited state biexcitons in the Varga's model is extremely important. This will allow us to fully understand the structures and formation mechanisms of these biexcitons and will enable us to overcome the limitations of previous experiments by engineering the environment of these biexcitons.

RESULTS AND DISCUSSION

Here, we successfully observed tightly bound biexcitons with a binding energy of ∼60 meV in atomically thin $MoSe_2$. The measured binding energy matches well with the theoretically predicted value of the excited state biexcitons in $MoSe_2$.[25] We further probed the formation dynamics of these biexcitons and found that the density of biexcitons increases with increasing density of negative trions and decreases with increasing density of excitons. This finding suggests that the biexcitons observed here are excited state biexcitons instead of ground state biexcitons. More importantly, we successfully triggered the emission of excited state biexcitons at room temperature in a freestanding bilayer $MoSe_2$ by modulating three independent parameters: (1) dielectric screening, (2) density of trions, and (3) excitation power. The implications of the tightly bound biexcitons at room temperature in 2D materials are far-reaching. It provides a room-temperature 2D platform to explore fundamental many-body interactions, which provides a route for quantum logical devices and entangled photon sources operating at room temperature.

It has been known that many-body effects,[26,27] which determine the behaviors of excitons, trions, and biexcitons, play important roles in optical transitions in low-dimensional

DOI: 10.1021/acsnano.7b03909
ACS Nano 2017, 11, 7468−7475

materials, including quantum wells, carbon nanotubes, 2D semiconductors, and so on.[8,11,26−37] Such a many-body effect, arising mainly from strong Coulomb interactions among charges, can be significantly enhanced with the reduction of dielectric screening from the environment[11,26,27,38] (Figure 1a,b). Thus, the biexciton or even higher-order multiple exciton states will typically become more pronounced in an environment with lower dielectric screening. To explore the dielectric screening effect on the many-body interactions in atomically thin semiconductors, we fabricated two types of $MoSe_2$ samples: SiO_2-supported and freestanding thin layers. The freestanding $MoSe_2$ sample was fabricated by mechanically transferring the sample onto a prepatterned circular hole on a SiO_2/Si substrate, as illustrated in Figure 1c. The freestanding atomically thin layers were confirmed by the contrast difference in optical microscope images (Figure 1d and Figure S1a) and the photoluminescence (PL) intensity difference in the PL mapping images (Figure 1e and Figure S1b). The layer number was identified and confirmed by phase-shifting interferometry[39] and PL spectroscopy measurements.

We compared the PL spectra of the $MoSe_2$ samples measured at 6 K and found that for the SiO_2-supported bilayer (2L) and monolayer (1L) $MoSe_2$ samples, there are only two distinct PL peaks at approximately 1.615 and 1.645 eV (Figure 1f and Figure S1c). These PL peaks can be identified as trion (T) and exciton (A) peaks according to previous studies.[10] Importantly, a new PL emission peak "X" at approximately 1.585 eV was observed from both the freestanding 2L (Figure 1f) and 1L (Figure S1d) $MoSe_2$ samples. We observed this new peak from multiple freestanding 1L and 2L $MoSe_2$ samples (more than 3 samples for each type). For some freestanding 2L $MoSe_2$ samples, this new peak became completely dominant in the PL spectrum, and the exciton (A) and trion (T) peaks were not pronounced at 6 K (Figure 2 and Figure S3), possibly because these samples had slightly different sample-dependent initial doping levels compared with the one shown in Figure 1f.

To determine the origin of this new peak X, we carried out power-dependent PL measurements on one freestanding 2L $MoSe_2$ sample at 6 K (Figure 2a). For a quantitative analysis, the integrated PL intensity of the X peak was plotted as a function of that of the exciton (A) peak (Figure 2b). By fitting the data with a power-law $I_X \propto I_A^{\alpha}$, where I_X is the integrated PL intensity of X peak and I_A is the integrated PL intensity of A peak,[11] it is found that peak X grows superlinearly with the excitation power ($\alpha \sim 1.23$). Based on the measured α value, peak X is attributed to the emission of biexcitons. In the ideal case, the α value of biexciton emission is expected to be close to 2; however, α values in the range of 1.2 to 1.9 were typically observed for biexciton emissions in quantum well systems[40,41] and TMD semiconductors[11,14] that might be due to the lack of thermal equilibrium between the states.[11]

Time-resolved PL (TRPL) measurement is another useful approach to identify the emission features in a PL spectrum. We measured the TRPL traces for the peaks A, T, and X (Figure 2c) at a temperature of 6 K. The decay trace curves were deconvoluted with respect to the instrument response and then were fitted with the equation $I = A\exp\left(-\frac{t}{\tau_1}\right) + B\exp\left(-\frac{t}{\tau_2}\right) + C$, where I is the PL intensity, A, B, and C are constants, t is time, and τ_1 is faster decay rate and τ_2 is the slower decay rate, indicating emission lifetimes for different decay processes.[42] The measured lifetimes of exciton (A), trion (T), and biexciton (X) were on the same

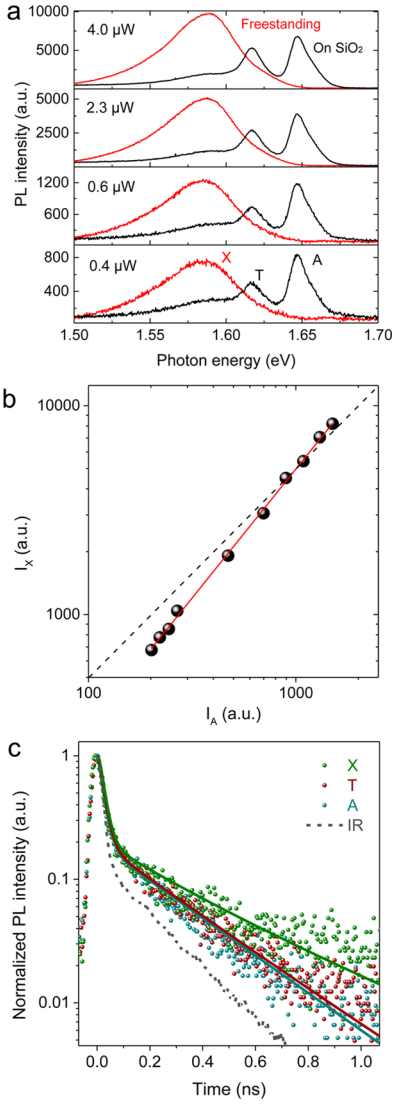

Figure 2. Power-dependent and time-resolved PL characterization. (a) Measured PL spectra from freestanding area (red lines) and SiO_2-supported area (black lines) under various excitation powers. (b) Log−log plot of integrated PL intensity of the peak X as a function of that of peak A. From the fitting curve, integrated PL intensity of the X peak grows superlinearly ($\alpha \sim 1.23$) with the increase of excitation power. (c) Measured time-resolved PL traces for A, T, and X peaks at a temperature of 6 K. IR represents instrument response curve. Based on the deconvolution with respect to the instrument response and a double exponential fit using the equation $I = A\exp\left(-\frac{t}{\tau_1}\right) + B\exp\left(-\frac{t}{\tau_2}\right) + C$, the fast decay lifetime τ_1 (and the corresponding amplitude A) values of exciton (A), trion (T), and biexciton (X) were extracted to be 8.7 (0.992), 9.8 (0.992), and 9.1 (0.988) ps, respectively; the slow decay lifetime τ_2 (and the corresponding amplitude B) values of exciton (A), trion (T), and biexciton (X) were extracted to be 292.8 (0.008), 322.6 (0.008), and 477.5 (0.012) ps, respectively.

order and comparable with each other, which is consistent with what has been reported in monolayer WSe_2,[11] indicating that the peak X is indeed from biexciton rather than localized exciton as the lifetime of localized exciton should be an order longer than that of the exciton and trion.[11] Moreover, the peaks A, T, and X from the freestanding 1L $MoSe_2$ sample (Figure S4) possess consistent lifetimes with the respective peaks in

DOI: 10.1021/acsnano.7b03909
ACS Nano 2017, 11, 7468−7475

freestanding 2L $MoSe_2$ (Figure 2d), which suggests the same emission features in both freestanding 1L and 2L $MoSe_2$ samples.

In addition, the spectrum of this new emission feature is asymmetric and can be fitted to two peaks, labeled as "X" and "L", by Lorentzian fitting (Figure S1d and Figure S2). The peak X is from the biexciton emission as discussed above, whereas the lower energy peak L could be from the contribution of defect states and is not the focus of this work. The measured full width at half-maximum (fwhm) value of the biexciton peak X in both freestanding 1L and 2L $MoSe_2$ samples was ~46 meV, which is similar to that of the biexciton peak observed in 1L WS_2.[14] From the temperature-dependent PL measurements (Figure S3a), we can clearly see that the intensity of the X peak increased dramatically as the temperature decreased from 63 to 6 K (Figure S3c).

Taken together, the observed power dependence and temporal dynamics properties of the X feature provide strong evidence for its assignment as a biexciton feature. We thus explored the binding energy of biexcitons and their dynamics to obtain a deeper physical insight into the biexcitons in atomically thin $MoSe_2$ layers. The binding energy of biexcitons is given by the energy difference between the exciton and biexciton peaks, assuming that an exciton is produced in the radiative decay of a biexciton.[11] The measured energy difference values between the X and A peaks in freestanding 1L and 2L $MoSe_2$ samples are 60 meV (Figure S1d) and 57 meV (Figure S2), respectively, which are considered to be the biexciton binding energies of $MoSe_2$. These values match very well with the calculated binding energy (58 meV) of an excited state biexciton in $MoSe_2$[25] (see Table 1). Freestanding 2L $MoSe_2$ has a biexciton binding energy slightly smaller than that of 1L $MoSe_2$, which might be due to the relatively larger screening in 2L $MoSe_2$. According to the theoretical model,[25] an excited state biexciton consists of a charge attached to a trion. The formation of an excited state biexciton state (TC) can be denoted as T + C → TC, where T is a trion and C is a charge. In great contrast, the calculated binding energy of a ground state biexciton (spatially symmetric exciton pairs, denoted as A + A → AA) in $MoSe_2$ is only 18 meV (Table 1), which is much smaller than the observed biexciton binding energy.

Table 1. Measured and Theoretically Calculated Binding Energies of Biexcitons in TMDs (meV)[a]

	MoS_2	$MoSe_2$	WS_2	WSe_2
theory (A + A)[25]	22	18	24	20
theory (T + C)[25]	69	58	67	59
experiments	70[12]	60[b]	65[13]	52[11]

[a]Note: T is a trion; C is a charge, and A is an exciton. [b]This work.

In addition to the binding energy difference, another way to differentiate the excited state and ground state biexcitons is to probe the dynamic relationship between the densities of biexcitons and trions. Based on the different formation mechanisms of these biexcitons, the density of excited state biexcitons should increase with the increase of trion density, whereas the density of ground state biexcitons should decrease because the formation of trions can reduce the density of excitons. Here, we successfully used an electrostatic doping technique to control the trion density in a 2L $MoSe_2$ metal-oxide-semiconductor (MOS) device (Figure S5) at 83 K, which leads to the dynamic modulation of biexciton emission (Figure 3).

First, we carried out the PL intensity mapping as a function of photon energy and gate voltage, using a relatively low excitation power of 264 μW (Figure 3a). Under a back gate voltage of 50 V, the negative trion (T) emission peak was dominant in the PL spectrum. At the same time, a new PL peak (labeled as X) at the low energy side appeared. When a negative back gate voltage of −50 V was applied, the exciton (A) emission peak became dominant and the new PL peak X disappeared (Figure 3a,c). To obtain a better insight, we generated the PL intensity mapping again using a relatively high excitation power of 602 μW (Figure 3b). The intensity of this new PL peak X increased much faster than the intensities of the exciton and trion peaks. Based on the superlinear increasing manner, this new PL peak X is assigned to the emission of biexcitons. From Figure 3b,d, we can clearly see that the density of biexcitons increases with increasing density of negative trions and decreases with increasing density of excitons. This further confirms that biexcitons observed here are excited state biexcitons (Figure 3e), instead of ground state biexcitons (Figure 3f). According to the calculation results by Varga *et al.*,[25] the binding energy of ground state biexcitons is only 18 meV, very close to the binding energy of trions. Therefore, it might not be possible to distinguish the ground state biexcitions and trions in experiments.[25] Also, excited state biexcitons are more likely to be observed in experiments than ground state biexctions because excited state biexcitons are energetically favorable and are spatially extended.[25] In addition, we only observed the emissions of excitons and trions but no emission of biexcitons in 1L $MoSe_2$ MOS devices at 83 K (Figure S6), which is consistent with a previous report.[10] The different PL behaviors in 2L and 1L $MoSe_2$ MOS devices are likely caused by the different trion densities in 2L and 1L $MoSe_2$ samples (as will be discussed later).

Due to thermally activated dissociation, biexcitons in both the freestanding $MoSe_2$ samples (Figure 1) and the 2L $MoSe_2$ MOS device (Figure 3) could only be observed at cryogenic temperatures (T < 100 K), which is similar to previously reported biexcitons in other TMD semiconductors.[11−14] The requirement of cryogenic temperature would significantly limit the potential applications of biexcitons. Fortunately, our experimental data (Figures 1−3) have shown that the probability of biexciton emissions in atomically thin $MoSe_2$ can be enhanced under the following three conditions (Figure 4a): (1) reduced dielectric screening, (2) enhanced density of trion states, and (3) high excitation laser power.

Here, we successfully demonstrated the emission of excited state biexcitons at room temperature in freestanding 2L $MoSe_2$ samples, in which those three parameters were all well-optimized (Figure 4). To achieve a clear comparison, we measured PL intensity mapping plots at room temperature as a function of photon energy and excitation power for four types of $MoSe_2$ systems (Figure 4b−e): freestanding 2L, freestanding 1L, SiO_2-supported 2L, and SiO_2-supported 1L. A biexciton emission feature at ~1.490 eV was observed only in the freestanding 2L $MoSe_2$ sample under relatively high excitation power at room temperature. To confirm the assignment of the biexciton peak in Figure 4b, we fitted the PL spectra and plotted the integrated intensities of the trion and biexciton peaks as a function of excitation power, as shown in Figure S7. At low excitation power, the trion peak (T) was dominant in the PL spectrum. With the growth of excitation power,

DOI: 10.1021/acsnano.7b03909
ACS Nano 2017, 11, 7468−7475

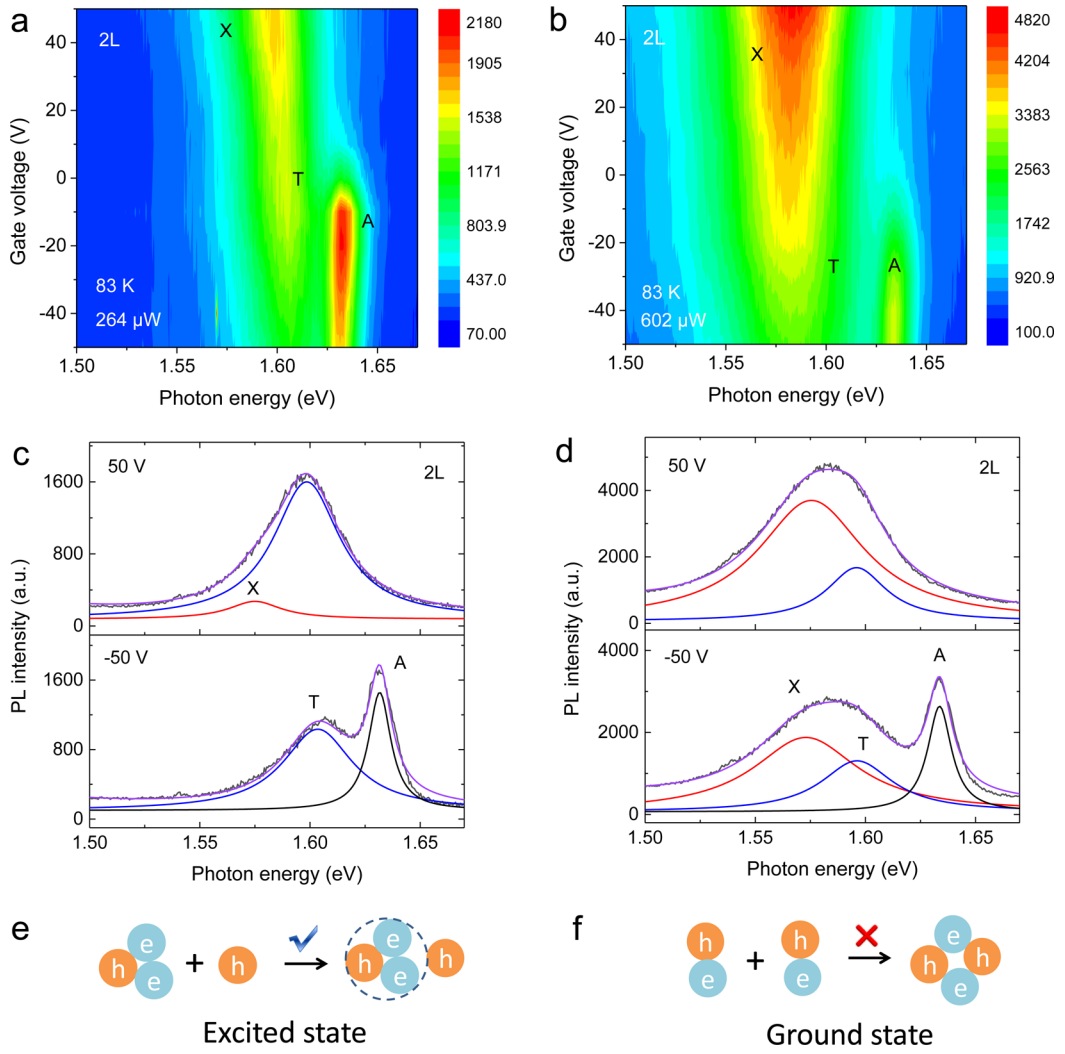

Figure 3. Electrostatic control of biexciton emissions. (a,b) PL intensity mapping as a function of photon energy and gate voltage from a 2L $MoSe_2$ metal-oxide-semiconductor (MOS) device measured at 83 K under different excitation power values of 264 (a) and 602 μW (b). Distinct exciton peaks show up as the back gate voltage goes from +50 to −50 V, indicating that trions in the bilayer $MoSe_2$ sample are negatively charged. (c,d) Measured PL spectra (gray lines) from the 2L $MoSe_2$ MOS device shown in a and b, respectively, under gate voltages of +50 and −50 V. The PL spectra are fitted to Lorentzian peaks, labeled as "X" (red line), "T" (blue line), and "A" (black line). Purple lines are the cumulative fitting results. (e,f) Schematic plots showing the formation process of excited state (e) and ground state biexcitons (f).

however, the intensity of the X peak increased much faster than that of the trion peak. Particularly, when the excitation power was lower than 50 μW, the integrated intensity of the trion and biexciton peaks increased as a function of power with exponent (α) values of ~0.85 and ~1.01, respectively. When the excitation power was higher than 50 μW, the X peak became dominant in the PL spectrum, and the α values of the trion and biexciton peaks became ~0.55 and ~1.41, respectively. The superlinear power dependence of this X peak further confirms its biexciton assignment. At high excitation power, the α value of the trion peak decreases, whereas that of the biexciton peak increases, which suggests the conversion of the trions to excited state biexcitons. In addition, the α value of the trion peak at room temperature was slightly less than 1, similar to the situation observed in other TMD semiconductors[11,14] due to the lack of full equilibrium.[8] On the other hand, the ratio of α values between biexciton and trion (1.41/0.55) increases dramatically when the excitation power is higher than 50 μW, suggesting that there might be a threshold value of trion density. Before the threshold, the transformation from trion to biexciton is restrained to some extent; beyond the threshold, the transformation from trion to biexciton start to dominate. In the power-dependent PL measurements, we used relatively low pumping power, and the power-induced spectral shifts of the exciton peaks in all freestanding and SiO_2-supported samples were less than 2.9 meV (Figures 4c,e and 3c,d), similar to the situation in a previous report.[11] This suggests that our pump laser has negligible heating effect on all the samples. The band gap renormalization effect can be ignored in Figure 4b, owing to the relatively low photodoping level (Supporting Information).

The reason why biexciton is observed in freestanding 2L instead of 1L $MoSe_2$ at room temperature could be explained as follows. The 1L $MoSe_2$ gives only one PL peak at ~1.562 eV from the emission of excitons at room temperature, whereas 2L $MoSe_2$ gives only one PL peak at ~1.520 eV from the emission of trions, which can be clearly observed from their temperature-dependent PL measurements (Figure S8a,b). This difference might be caused by the relatively low initial doping levels in $MoSe_2$ crystals[10] and the different band gap nature in 1L and

DOI: 10.1021/acsnano.7b03909
ACS Nano 2017, 11, 7468−7475

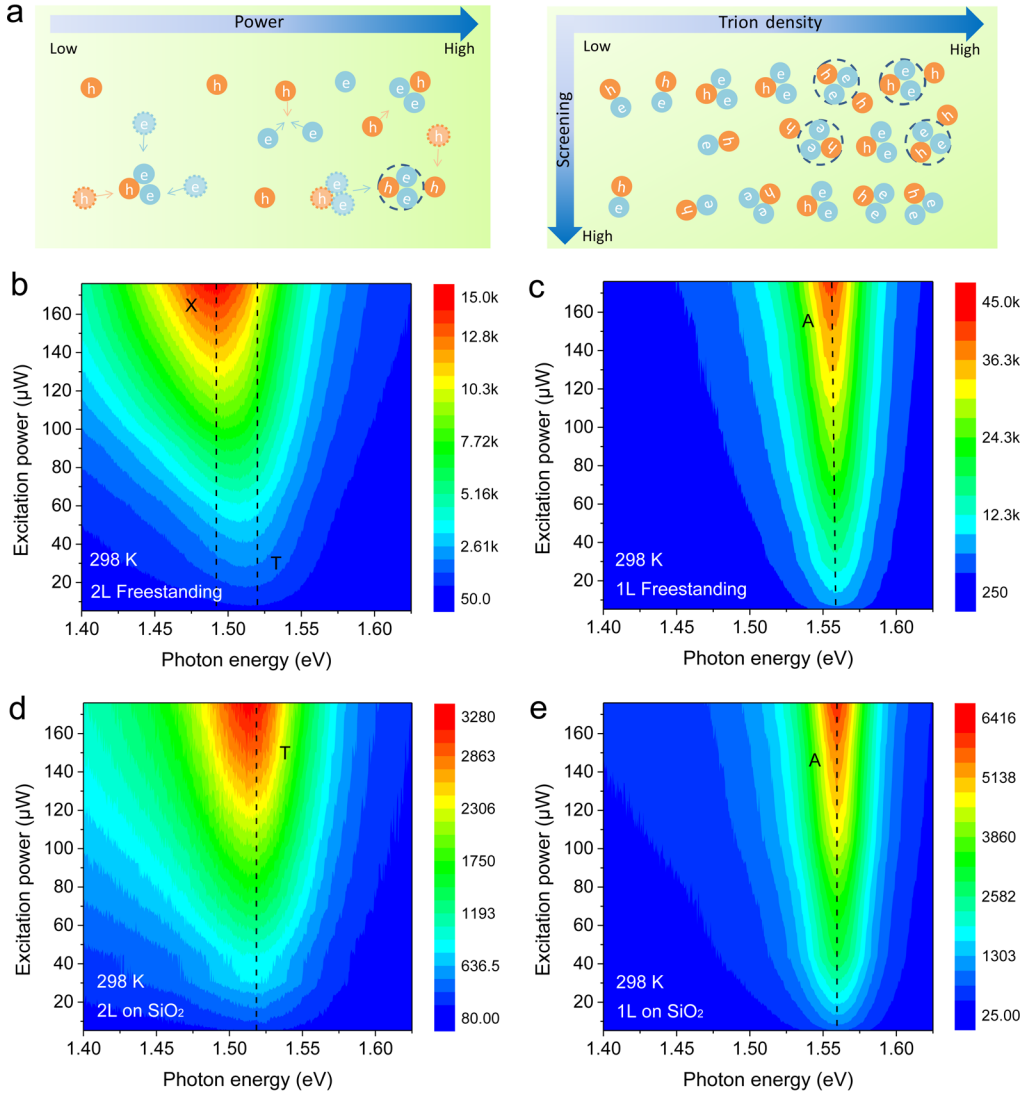

Figure 4. Excited state biexciton engineering at room temperature in atomically thin $MoSe_2$. (a) Schematic plots showing that the density of excited state biexciton will be enhanced with lower dielectric screening, higher density of trions, and higher excitation power. (b–e) Measured PL intensity mapping plots at room temperature as a function of photon energy and excitation power for four types of $MoSe_2$ samples: freestanding 2L (b), freestanding 1L (c), SiO_2-supported 2L and (d), SiO_2-supported 1L (e).

2L $MoSe_2$ samples. The 1L $MoSe_2$ possesses a direct band gap and thus a relatively balanced distribution of thermal charges in the K–K valleys of the band structure, where the PL transitions occur. In contrast, 2L $MoSe_2$ possesses an indirect band gap and thus an unbalanced thermal charge distribution in the K–K valleys, which leads to a higher trion density (Figure S8c,d). Therefore, at room temperature, a freestanding 2L $MoSe_2$ sample possesses low dielectric screening and high trion density, which leads to the emission of excited state biexcitons under a relatively high excitation power. The demonstrated capability of biexciton engineering at room temperature in $MoSe_2$ will allow us to explore fundamental many-body interactions in a simplified room-temperature 2D platform, which will enable a class of quantum devices such as bright entangled and correlated photon sources operating at room temperature.[21] In addition, based on theoretical calculations, biexitons have a radius larger than that of excitons and trions in 2D TMDs (Supporting Information). Because of the larger separation between charges in biexcitons, the Coulomb interactions of biexcitons are more likely to be influenced by dielectric screening of the external media than those of trions in TMDs.[11]

CONCLUSIONS

In conclusion, we observed tightly bound excited state biexcitons with a binding energy of ~60 meV in atomically thin $MoSe_2$, which was confirmed by both the agreement of experimental and theoretical values of the binding energy and the observed formation dynamics of these excited state biexcitons. We also found that the emission from these excited state biexcitons in atomically thin $MoSe_2$ strongly relies on three important conditions: reduced dielectric screening, high density of trions, and high excitation power. By optimizing those three conditions, we successfully triggered the emission of excited state biexcitons in freestanding 2L $MoSe_2$ samples at room temperature. Our findings will provide a platform to explore fundamental many-body interactions in atomically thin semiconductors. We envisage that such a 2D platform can form the basis of bright quantum sources of entangled and correlated photons, thus enabling a class of ultrafast optoelectronics and

DOI: 10.1021/acsnano.7b03909
ACS Nano 2017, 11, 7468–7475

quantum devices with applications in quantum communications and cryptography.

METHODS

Device Fabrication and Characterization. Mechanical exfoliation was used to dry transfer 1L and 2L $MoSe_2$ flakes onto the SiO_2/Si substrate (a 275 nm layer of thermal oxide on n^+-doped silicon), near the prepatterned Au electrode for those MOS devices. The Au electrodes were patterned by conventional photolithography, metal deposition, and lift-off processes. Another thick graphite flake was similarly transferred to electrically bridge the $MoSe_2$ flake and the Au electrode, forming a MOS device. For the suspended samples, 1L and 2L $MoSe_2$ samples were dry transferred onto a 275 nm SiO_2/Si substrate with pre-etched 3 μm deep holes.

Optical Characterizations. PL measurements at room temperature and 83 K were conducted using a Horiba JobinYvon T64000 micro-Raman system equipped with charge-coupled device (CCD) and InGaAs detectors, along with a 532 nm Nd:YAG laser as the excitation source. For low-temperature (down to 83 K) measurements, the sample was placed into a microscope-compatible chamber with a low-temperature controller (using liquid nitrogen as the coolant). Micro-PL spatial mapping was performed using a commercial WiTec alpha300S system in the scanning confocal microscope configuration. The power-dependent PL measurements at 6 K and TRPL measurements were conducted in a setup that incorporates micro-PL spectroscopy with a time-correlated single-photon counting (TCSPC) system and uses liquid helium as the coolant. A linearly polarized pulsed laser (frequency doubled to 522 nm, with a 300 fs pulse width and a 20.8 MHz repetition rate) was directed to a high numerical aperture (NA = 0.7) objective (Nikon S Plan 60×). The PL signal was collected by a grating spectrometer, thereby either recording the PL spectrum through the CCD (Princeton Instruments, PIXIS) or detecting the PL intensity decay by a Si single photon avalanche diode and the TCSPC (PicoHarp 300) system with a resolution of 20 ps. All the PL spectra were corrected for the instrument response. Electrical bias was applied using a Keithley 4200 semiconductor analyzer.

Simulations. First-principle calculations based on the density functional theory were used to calculate band diagrams of 1L and 2L $MoSe_2$. The scissor operator was used to correct the band gaps to GW approximation values.

ASSOCIATED CONTENT

Supporting Information

The Supporting Information is available free of charge on the ACS Publications website at DOI: 10.1021/acsnano.7b03909.

Details of additional experimental PL measurement results and data analysis (PDF)

AUTHOR INFORMATION

Corresponding Author

*E-mail: yuerui.lu@anu.edu.au.

ORCID

Qinghua Qin: 0000-0003-0948-784X
Dragomir Neshev: 0000-0002-4508-8646
Yuerui Lu: 0000-0001-6131-3906

Author Contributions

Y.L. designed the project; J.P. carried out sample mechanical exfoliation and microscope imaging; J.Y. and J.P. carried out the PL measurements; F.W., S.M., H.T., and C.J. built the setup for PL measurements; D.N. built the setup for micro-PL mapping; T.L. and J.-C.Z. conducted the DFT calculations; J.P., Y.L., and J.Y. analyzed the data and prepared the manuscript; all authors contributed to the manuscript. J.P. and J.Y. contributed equally to this work.

Notes

The authors declare no competing financial interest.

ACKNOWLEDGMENTS

We would like to acknowledge the facility support from the ACT node of the Australian National Fabrication Facility (ANFF). We also acknowledge financial support from ANU Ph.D. student scholarship, China Scholarship Council, ANU Major Equipment Committee fund (No. 14MEC34), Australian Research Council (ARC) Discovery Early Career Researcher Award (DECRA) DE140100805, ARC Discovery Project (DP150103733), the Natural Science Foundation of Fujian Province, China (Grant No. 2015J01029), and Special Program for Applied Research on Super Computation of the NSFC-Guangdong Joint Fund (the second phase).

REFERENCES

(1) Britnell, L.; Ribeiro, R. M.; Eckmann, A.; Jalil, R.; Belle, B. D.; Mishchenko, A.; Kim, Y.-J.; Gorbachev, R. V.; Georgiou, T.; Morozov, S. V.; Grigorenko, A. N.; Geim, A. K.; Casiraghi, C.; Neto, A. H. C.; Novoselov, K. S. Strong Light-Matter Interactions in Heterostructures of Atomically Thin Films. *Science* **2013**, *340*, 1311−1314.

(2) Yang, J.; Wang, Z.; Wang, F.; Xu, R.; Tao, J.; Zhang, S.; Qin, Q.; Luther-Davies, B.; Jagadish, C.; Yu, Z.; Lu, Y. Atomically Thin Optical Lenses and Gratings. *Light: Sci. Appl.* **2016**, *5*, e16046.

(3) Lopez-Sanchez, O.; Lembke, D.; Kayci, M.; Radenovic, A.; Kis, A. Ultrasensitive Photodetectors Based on Monolayer MoS_2. *Nat. Nanotechnol.* **2013**, *8*, 497−501.

(4) Ye, Y.; Wong, Z. J.; Lu, X.; Ni, X.; Zhu, H.; Chen, X.; Wang, Y.; Zhang, X. Monolayer Excitonic Laser. *Nat. Photonics* **2015**, *9*, 733−737.

(5) Chen, H.; Corboliou, V.; Solntsev, A. S.; Choi, D.-Y.; Vincenti, M. A.; de Ceglia, D.; De Angelis, C.; Lu, Y.; Neshev, D. N. Enhanced Second-Harmonic Generation from Two-Dimensional $MoSe_2$ on a Silicon Waveguide. *Light Sci. Appl.* **2017**, *6*, e17060.

(6) Chen, H.; Yang, J.; Rusak, E.; Straubel, J.; Guo, R.; Myint, Y. W.; Pei, J.; Decker, M.; Staude, I.; Rockstuhl, C.; Lu, Y.; Kivshar, Y. S.; Neshev, D. Manipulation of Photoluminescence of Two-Dimensional $MoSe_2$ by Gold Nanoantennas. *Sci. Rep.* **2016**, *6*, 22296.

(7) Zhu, Y.; Yang, J.; Zhang, S.; Mokhtar, S.; Pei, J.; Wang, X.; Lu, Y. Strongly Enhanced Photoluminescence in Nanostructured Monolayer MoS_2 by Chemical Vapor Deposition. *Nanotechnology* **2016**, *27*, 135706.

(8) He, K.; Kumar, N.; Zhao, L.; Wang, Z.; Mak, K. F.; Zhao, H.; Shan, J. Tightly Bound Excitons in Monolayer WSe_2. *Phys. Rev. Lett.* **2014**, *113*, 026803.

(9) Mak, K. F.; He, K.; Lee, C.; Lee, G. H.; Hone, J.; Heinz, T. F.; Shan, J. Tightly Bound Trions in Monolayer MoS_2. *Nat. Mater.* **2012**, *12*, 207−211.

(10) Ross, J. S.; Wu, S.; Yu, H.; Ghimire, N. J.; Jones, A. M.; Aivazian, G.; Yan, J.; Mandrus, D. G.; Xiao, D.; Yao, W.; Xu, X. Electrical Control of Neutral and Charged Excitons in a Monolayer Semiconductor. *Nat. Commun.* **2013**, *4*, 1474.

(11) You, Y.; Zhang, X.-X.; Berkelbach, T. C.; Hybertsen, M. S.; Reichman, D. R.; Heinz, T. F. Observation of Biexcitons in Monolayer WSe_2. *Nat. Phys.* **2015**, *11*, 477−481.

(12) Mai, C.; Barrette, A.; Yu, Y.; Semenov, Y. G.; Kim, K. W.; Cao, L.; Gundogdu, K. Many-Body Effects in Valleytronics: Direct Measurement of Valley Lifetimes in Single-Layer MoS_2. *Nano Lett.* **2014**, *14*, 202−206.

(13) Plechinger, G.; Nagler, P.; Kraus, J.; Paradiso, N.; Strunk, C.; Schüller, C.; Korn, T. Identification of Excitons, Trions and Biexcitons in Single-Layer WS_2. *Phys. Status Solidi RRL* **2015**, *9*, 457−461.

(14) Shang, J.; Shen, X.; Cong, C.; Peimyoo, N.; Cao, B.; Eginligil, M.; Yu, T. Observation of Excitonic Fine Structure in a 2D Transition-Metal Dichalcogenide Semiconductor. *ACS Nano* **2015**, *9*, 647−655.

DOI: 10.1021/acsnano.7b03909
ACS Nano 2017, 11, 7468−7475

(15) Soavi, G.; Dal Conte, S.; Manzoni, C.; Viola, D.; Narita, A.; Hu, Y.; Feng, X.; Hohenester, U.; Molinari, E.; Prezzi, D.; Mullen, K.; Cerullo, G. Exciton-Exciton Annihilation and Biexciton Stimulated Emission in Graphene Nanoribbons. *Nat. Commun.* **2016**, *7*, 11010.
(16) Chen, G.; Stievater, T. H.; Batteh, E. T.; Li, X.; Steel, D. G.; Gammon, D.; Katzer, D. S.; Park, D.; Sham, L. J. Biexciton Quantum Coherence in a Single Quantum Dot. *Phys. Rev. Lett.* **2002**, *88*, 117901.
(17) Pedersen, T. G.; Pedersen, K.; Cornean, H. D.; Duclos, P. Stability and Signatures of Biexcitons in Carbon Nanotubes. *Nano Lett.* **2005**, *5*, 291−294.
(18) Li, X.; Wu, Y.; Steel, D.; Gammon, D.; Stievater, T. H.; Katzer, D. S.; Park, D.; Piermarocchi, C.; Sham, L. J. An All-Optical Quantum Gate in a Semiconductor Quantum Dot. *Science* **2003**, *301*, 809−811.
(19) Grim, J. Q.; Christodoulou, S.; Di Stasio, F.; Krahne, R.; Cingolani, R.; Manna, L.; Moreels, I. Continuous-Wave Biexciton Lasing at Room Temperature Using Solution-Processed Quantum Wells. *Nat. Nanotechnol.* **2014**, *9*, 891−895.
(20) Masumoto, Y.; Kawamura, T.; Era, K. Biexciton Lasing in CuCl Quantum Dots. *Appl. Phys. Lett.* **1993**, *62*, 225−227.
(21) Shields, A. J. Semiconductor Quantum Light Sources. *Nat. Photonics* **2007**, *1*, 215−223.
(22) Klingshirn, C. F. *Semiconductor Optics*; Springer: Berlin, 2007; Vol. 3.
(23) Velizhanin, K. A.; Saxena, A. Excitonic Effects in Two-Dimensional Semiconductors: Path Integral Monte Carlo Approach. *Phys. Rev. B: Condens. Matter Mater. Phys.* **2015**, *92*, 195305.
(24) Riva, C.; Peeters, F. M.; Varga, K. Excitons and Charged Excitons in Semiconductor Quantum Wells. *Phys. Rev. B: Condens. Matter Mater. Phys.* **2000**, *61*, 13873−13881.
(25) Zhang, D. K.; Kidd, D. W.; Varga, K. Excited Biexcitons in Transition Metal Dichalcogenides. *Nano Lett.* **2015**, *15*, 7002−7005.
(26) Qiu, D. Y.; da Jornada, F. H.; Louie, S. G. Optical Spectrum of MoS_2: Many-Body Effects and Diversity of Exciton States. *Phys. Rev. Lett.* **2013**, *111*, 216805.
(27) Molina-Sánchez, A.; Sangalli, D.; Hummer, K.; Marini, A.; Wirtz, L. Effect of Spin-Orbit Interaction on the Optical Spectra of Single-Layer, Double-Layer, and Bulk MoS_2. *Phys. Rev. B: Condens. Matter Mater. Phys.* **2013**, *88*, 045412.
(28) Perebeinos, V.; Tersoff, J.; Avouris, P. Scaling of Excitons in Carbon Nanotubes. *Phys. Rev. Lett.* **2004**, *92*, 257402.
(29) Kulik, L. V.; Kulakovskii, V. D.; Bayer, M.; Forchel, A.; Gippius, N. A.; Tikhodeev, S. G. Dielectric Enhancement of Excitons in near-Surface Quantum Wells. *Phys. Rev. B: Condens. Matter Mater. Phys.* **1996**, *54*, R2335−R2338.
(30) Yang, J.; Lü, T.; Myint, Y. W.; Pei, J.; Macdonald, D.; Zheng, J.-C.; Lu, Y. Robust Excitons and Trions in Monolayer $MoTe_2$. *ACS Nano* **2015**, *9*, 6603−6609.
(31) Xu, R.; Yang, J.; Myint, Y. W.; Pei, J.; Yan, H.; Wang, F.; Lu, Y. Exciton Brightening in Monolayer Phosphorene *via* Dimensionality Modification. *Adv. Mater.* **2016**, *28*, 3493−3498.
(32) Xu, R.; Zhang, S.; Wang, F.; Yang, J.; Wang, Z.; Pei, J.; Myint, Y. W.; Xing, B.; Yu, Z.; Fu, L.; Qin, Q.; Lu, Y. Extraordinarily Bound Quasi-One-Dimensional Trions in Two-Dimensional Phosphorene Atomic Semiconductors. *ACS Nano* **2016**, *10*, 2046−2053.
(33) Zhang, S.; Yang, J.; Xu, R.; Wang, F.; Li, W.; Ghufran, M.; Zhang, Y.-W.; Yu, Z.; Zhang, G.; Qin, Q.; Lu, Y. Extraordinary Photoluminescence and Strong Temperature/Angle-Dependent Raman Responses in Few-Layer Phosphorene. *ACS Nano* **2014**, *8*, 9590−9596.
(34) Xu, R.; Yang, J.; Zhu, Y.; Yan, H.; Pei, J.; Myint, Y. W.; Zhang, S.; Lu, Y. Layer-Dependent Surface Potential of Phosphorene and Anisotropic/Layer-Dependent Charge Transfer in Phosphorene−Gold Hybrid Systems. *Nanoscale* **2016**, *8*, 129−135.
(35) Lu, J.; Yang, J.; Carvalho, A.; Liu, H.; Lu, Y.; Sow, C. H. Light−Matter Interactions in Phosphorene. *Acc. Chem. Res.* **2016**, *49*, 1806−1815.
(36) Pei, J.; Gai, X.; Yang, J.; Wang, X.; Yu, Z.; Choi, D.-Y.; Luther-Davies, B.; Lu, Y. Producing Air-Stable Monolayers of Phosphorene and Their Defect Engineering. *Nat. Commun.* **2016**, *7*, 10450.
(37) Pei, J.; Yang, J.; Xu, R.; Zeng, Y.-H.; Myint, Y. W.; Zhang, S.; Zheng, J.-C.; Qin, Q.; Wang, X.; Jiang, W.; Lu, Y. Exciton and Trion Dynamics in Bilayer MoS_2. *Small* **2015**, *11*, 6384−6390.
(38) Lin, Y.; Ling, X.; Yu, L.; Huang, S.; Hsu, A. L.; Lee, Y.-H.; Kong, J.; Dresselhaus, M. S.; Palacios, T. Dielectric Screening of Excitons and Trions in Single-Layer MoS_2. *Nano Lett.* **2014**, *14*, 5569−5576.
(39) Yang, J.; Xu, R. J.; Pei, J. J.; Myint, Y. W.; Wang, F.; Wang, Z.; Zhang, S.; Yu, Z. F.; Lu, Y. R. Optical Tuning of Exciton and Trion Emissions in Monolayer Phosphorene. *Light: Sci. Appl.* **2015**, *4*, e312.
(40) Phillips, R. T.; Lovering, D. J.; Denton, G. J.; Smith, G. W. Biexciton Creation and Recombination in a Gaas Quantum Well. *Phys. Rev. B: Condens. Matter Mater. Phys.* **1992**, *45*, 4308−4311.
(41) Birkedal, D.; Singh, J.; Lyssenko, V. G.; Erland, J.; Hvam, J. M. Binding of Quasi-Two-Dimensional Biexcitons. *Phys. Rev. Lett.* **1996**, *76*, 672−675.
(42) Liu, X.; Yu, H.; Ji, Q.; Gao, Z.; Ge, S.; Qiu, J.; Liu, Z.; Zhang, Y.; Sun, D. An Ultrafast Terahertz Probe of the Transient Evolution of the Charged and Neutral Phase of Photo-Excited Electron-Hole Gas in a Monolayer Semiconductor. *2D Mater.* **2016**, *3*, 014001.

DOI: 10.1021/acsnano.7b03909
ACS Nano 2017, 11, 7468−7475